Optics & Laser Technology 143 (2021) 107375

Contents lists available at ScienceDirect

Optics and Laser Technology

journal homepage: www.elsevier.com/locate/optlastec

Broadband multimodal THz waveguides for efficient transfer of high-power radiation in space-confined conditions

Anatoly R. Melnikov [a,b,c,*], Arkady A. Samsonenko [b,c], Yaroslav V. Getmanov [c,d], Oleg A. Shevchenko [d], Darya A. Shevchenko [d], Alexander A. Stepanov [a], Matvey V. Fedin [b,c], Maxim A. Yurkin [a,c], Sergey L. Veber [b,c,*]

[a] Voevodsky Institute of Chemical Kinetics and Combustion of the Siberian Branch of the Russian Academy of Sciences, 3, Institutskaya Str., Novosibirsk 630090, Russia
[b] International Tomography Center of the Siberian Branch of the Russian Academy of Sciences, 3a, Institutskaya Str., Novosibirsk 630090, Russia
[c] Novosibirsk State University, 1, Pirogova Str., Novosibirsk 630090, Russia
[d] Budker Institute of Nuclear Physics of the Siberian Branch of the Russian Academy of Sciences, 11, Acad. Lavrentieva Ave., Novosibirsk 630090, Russia

ARTICLE INFO

Keywords:
THz radiation
Broadband multimodal THz waveguide
Hollow metal/dielectric waveguide
EPR spectroscopy
Free electron laser
Single-molecule magnet

ABSTRACT

Terahertz (THz) range, which lies between the microwave and infrared regions of the electromagnetic spectrum, presents a new frontier containing an abundance of technical applications and fundamental research problems. There are several challenges limiting the progress in the THz science and technology. One of them is the limited range of the guided-wave propagation of THz radiation, owing to the high loss from the finite conductivity of metals and the high absorption coefficient of dielectric materials in the THz range. In this work, we discuss the design and fabrication of multimodal hollow THz waveguides used at the X-band Electron Paramagnetic Resonance (EPR) endstation located at the Novosibirsk Free Electron Laser facility (NovoFEL). Experiments carried out at the EPR endstation are aimed to investigate the impact of THz and far infrared radiation on the spin system of different inorganic complexes and organic radicals. The EPR probehead and cryostat impose strict constraints on the possible ways of transferring the THz radiation to the sample, requiring the development, manufacturing, and characterization of specific waveguides. The proposed waveguides for X-band EPR measurements under THz radiation resemble hollow metal/dielectric waveguides. They have the shape of a hollow cylinder, tapering towards the end, with a silver-coated inner surface, and allow THz radiation to be transmitted over a distance of about 60 cm in a wide frequency range from THz to middle infrared. The waveguides performance was characterized at different frequencies of NovoFEL radiation and compared with numerical simulations. Following the requirements of polarization-sensitive EPR experiments, the waveguides were further modified by a miniature attachment, consisting of a polarizer, a semiconductor mirror, and a quarter-wave plate. The attachment allows preserving the initial polarization properties of THz radiation, turns its propagation vector, and creates the circular-polarized light irradiating the sample – all inside the limited volume of the EPR probehead.

1. Introduction

The far infrared region of the electromagnetic spectrum (0.1–10 THz), known as the terahertz (THz) frequency range, is a scientifically rich spectral window that is currently served by limited technology [1–4]. The main issues holding back the development of THz based science include (i) the lack of intense THz sources and sensitive THz detectors, (ii) strong water vapors absorption that prevents imaging of water-rich objects and limits the range of THz wave propagation, (iii) lack of effective waveguides for transmitting THz radiation over long distances.

THz radiation can be transferred for a long distance as a Gaussian beam with relatively big aperture of tens to hundreds of wavelengths [5]. With an appropriate aperture, the main propagation losses of THz radiation in such radiation beamline are often caused by absorption of the medium inside the beamline. To tackle this issue a carefully dried medium is typically used, allowing to reach almost complete transmittance of the THz radiation in the transmission windows of the water vapor spectrum [5]. Unlike for large-size radiation beamlines, inside the experimental setup the THz beampath is usually restricted in the

* Corresponding authors.
E-mail addresses: anatoly.melnikov@tomo.nsc.ru (A.R. Melnikov), sergey.veber@tomo.nsc.ru (S.L. Veber).

https://doi.org/10.1016/j.optlastec.2021.107375
Received 12 May 2021; Accepted 27 June 2021
Available online 10 July 2021

aperture, assuming the use of THz waveguides or a specially designed optical system, which is mounted in the dried atmosphere [6–8]. For the design and manufacture of THz waveguides, standard microwave and optical technologies could be used, but they are considerably affected by the relatively strong absorption in most of the conventional waveguide structures, preventing THz wave transmission over long distances [9–13]. To date, many THz waveguides have been proposed, such as hollow metal waveguides [14], metal-wire waveguides [15], dielectric tube waveguides [16–19], hollow metal/dielectric waveguides [20,21], parallel plate waveguides [22,23], photonic crystal fibers [24,25], and metamaterial cladding hollow-core fibers [26,27]. Among them, flexible hollow metal/dielectric waveguides (HMWs) are becoming increasingly attractive today due to their easy fabrication, simple design, and the ability to control the transmission loss at the target frequency by varying the thickness of the dielectric layer [28,29]. In addition to its primary characteristic – radiation transmission efficiency – THz waveguides usually have other constraints on their geometric, magnetic, thermal, and electric-conductivity properties. Meeting all such requirements, THz waveguides play an important role in the overall performance of experimental setups. Their design, manufacture, and characterization are often critical to understanding the optimal approaches to perform different types of experiments.

In this paper, we propose a design and report a performance study for home-built hollow waveguides used for X-band (9 GHz) Electron Paramagnetic Resonance (EPR) measurements when the sample is irradiated with high-power THz pulses. The design of the waveguides resembles HMWs in which no dielectric layer is used and a reflective silver layer is coated directly on inflexible base with a circular cross-section. The X-band EPR spectroscopy endstation is located at the Novosibirsk Free Electron Laser (NovoFEL) facility and operates in both continuous-wave and time-resolved modes, allowing detection of either direct or indirect influence of pulsed NovoFEL radiation on the spin system under study [30,31]. The NovoFEL facility has three free electron lasers that produce high-power tunable laser radiation in the middle infrared (1040–1170 cm^{-1}), far infrared (110–285 cm^{-1}), and terahertz (30–110 cm^{-1}) frequency ranges [32–34]. NovoFEL can operate in both quasi-continuous and pulsed modes with an average power of up to 200 W. In the continuous mode, the radiation consists of a periodic train of pulses with duration of several tens of picoseconds. The pulse mode allows generating THz macropulses of various durations containing a sequence of individual picoseconds pulses [35]. The properties of the NovoFEL radiation, namely a wide frequency range and high average power, as well as the geometrical constraints of the EPR probehead significantly limit the possibility of utilizing standard quasi-optical or quasi-microwave waveguides, requiring the use of a specially designed multimodal waveguide with circular cross-section. In contrast to the HMWs described in the literature, the waveguides proposed in this work are not tuned to one radiation frequency and have reasonable transmission losses over the entire frequency range of NovoFEL radiation.

Sections of the article include a description of the X-band EPR probehead and proposed THz waveguides, as well as the results of measurements and numerical simulations of their transmission coefficient and polarization degree.

2. Construction of the EPR probehead

Experimental methods of EPR spectroscopy are typically based on the use of different microwave resonators. For X-band (9 GHz) setups the main types include rectangular cavities, loop-gap [36,37] and dielectric resonators [38,39]. The latter typically provides high Q-value and high efficiency of spatial separation of magnetic and electric components of the applied microwave field, allowing the study of the samples with high dielectric losses and giving rise to the widespread use of this type of resonators in home-built and commercial EPR apparatus [38,39].

The X-band EPR endstation of NovoFEL is equipped with a dielectric resonator Bruker ER 4118X-MD-5 W1 (MD-5, Bruker, Germany). It is based on the sapphire dielectric cylinder with an outer diameter of 10 mm and a hole of 5 mm. It has high Q-value of about 30000 at 6 K [38] and large sample access of 5 mm. The schematic representation of the MD-5 is shown in Fig. 1a. Since most experiments are carried out at low temperature, the resonator is placed inside a helium cryostat (Cryotrade Engineering, Russia). The MD-5 resonator provides an easy and comfortable way to exchange the samples. The sample is fixed on a sample rod that can be easily extracted from the resonator. The entire procedure to change the sample takes less than a couple of minutes even if the sample is at helium temperature.

There are two main options to irradiate a sample of interest inside the MD-5. The first is to direct radiation from the top, combining the sample holder with the waveguide. The second is to radiate the sample perpendicularly to the long axis of the resonator via the quartz window in the cryostat. Both options and the standard EPR sample holder (a rod of 56 cm length and 8 mm in diameter) are shown in Fig. 1.

In the case of visible, near ultraviolet, or near infrared radiation both possibilities of radiation transfer can be implemented, using standard optical elements (optical path 2 in Fig. 1b) or quartz optic fiber, combined with the sample holder (optical path 1 in Fig. 1a, 1b). For far infrared and terahertz radiation, the only reasonable way is to direct radiation from the top, since optical elements used in the cryostat and EPR resonator are not transparent in certain ranges of the specified frequencies [40]. This option implies combining the waveguide with the sample holder. In such a case, the waveguide allows controlling the divergence rate of radiation and cuts off the humid atmosphere, replacing it with the inert media inside the cryostat (helium or nitrogen gas).

3. Multimodal terahertz waveguides

Size restrictions imposed by the resonator, strong divergence of the radiation of the far infrared and THz frequency range, as well as high average power of NovoFEL radiation limit the approaches for designing an efficient terahertz waveguide. As it was mentioned in the previous section, the most straightforward way is to deliver radiation from the top, combining the functions of the waveguide and the sample holder. The following subsections discuss the general procedure for designing and fabricating a THz multimodal waveguide for the EPR endstation of NovoFEL.

3.1. Waveguide design

In order to combine an EPR sample holder and the terahertz waveguide, a device should have a form of long hollow cylinder tapering towards the end. Proposed form mimics a standard sample holder and matches the inner diameter of the working area of the resonator – inner area of sapphire hollow cylinder. According to the resonator size, tapering should be done from 8 mm to approximately 3–4 mm in outer diameter. The inner diameter of the THz waveguide should be as large as possible. There are two main possibilities to achieve mentioned requirements: (i) 8 mm long cylinder ending by a long (up to 5–6 cm) gradual tapering, (ii) a combination of two cylinders 8 and 3.5 mm in outer diameter, respectively, combined by a relatively short and steep tapering region (2–3 cm). The latter tapering can also be considered gradual, since the tapering angle does not exceed 6° (calculated from the above dimensions). However, we will further use the terms “gradual” and “steep” to distinguish these two options – see Fig. 2 for more details. The two proposed waveguide designs were empirically compared in terms of their transmission coefficients and polarization degrees in the three frequency ranges available for NovoFEL. These waveguides also have a small (approximately 0.5–1 mm in diameter) ventilation hole located at a distance of 8–10 cm from the end of the waveguide. This hole is used to replace the normal atmosphere inside the waveguide with an inert helium or nitrogen cryostat atmosphere, when the waveguide is inserted into the latter.

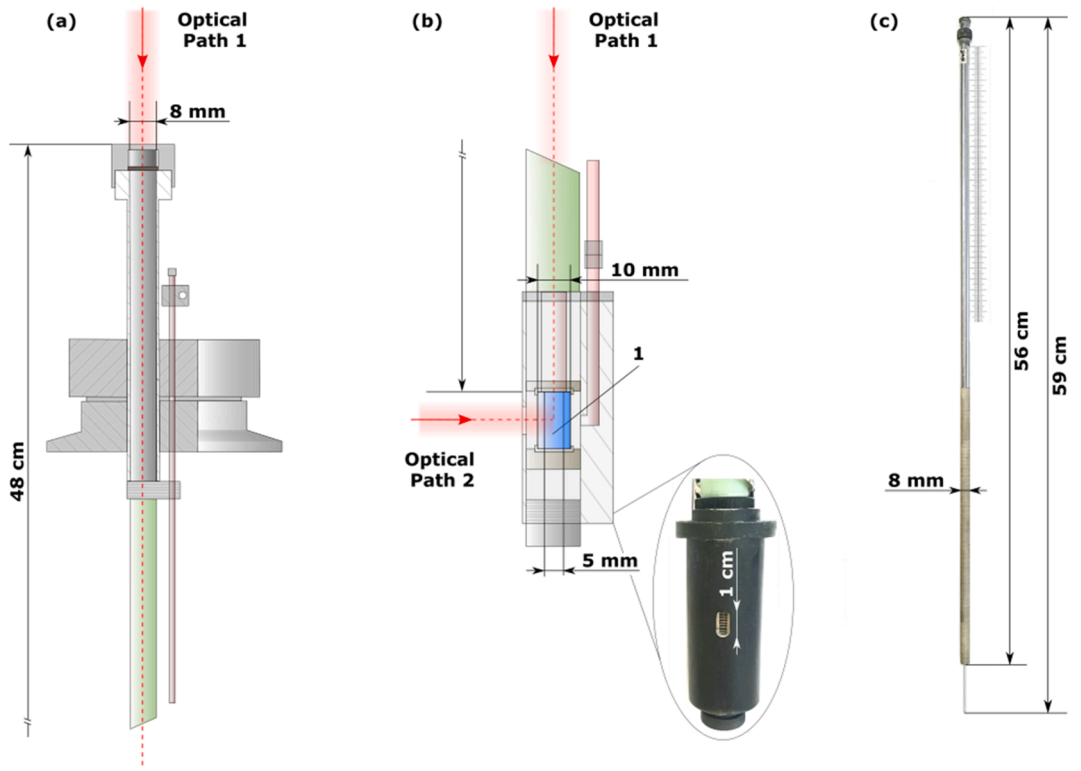

Fig. 1. (a) Schematic representation of the upper part of the MD-5 dielectric resonator. Proportions are exaggerated. A possible way of sample irradiation from the top is shown as optical path 1; (b) Schematic representation of the lower part of the MD-5 dielectric resonator. Proportions are exaggerated. Two possible ways of sample irradiation are shown as optical path 1 (from the top) and optical path 2 (via the quartz window in the cryostat), respectively. Number 1 indicates sapphire hollow cylinder, fixed in polytetrafluoroethylene inserts. The inset shows the photograph of the front view of the lower part with a window for ultraviolet or visible irradiation of the sample. (c) Photograph of the standard sample holder for EPR measurements with its dimensions.

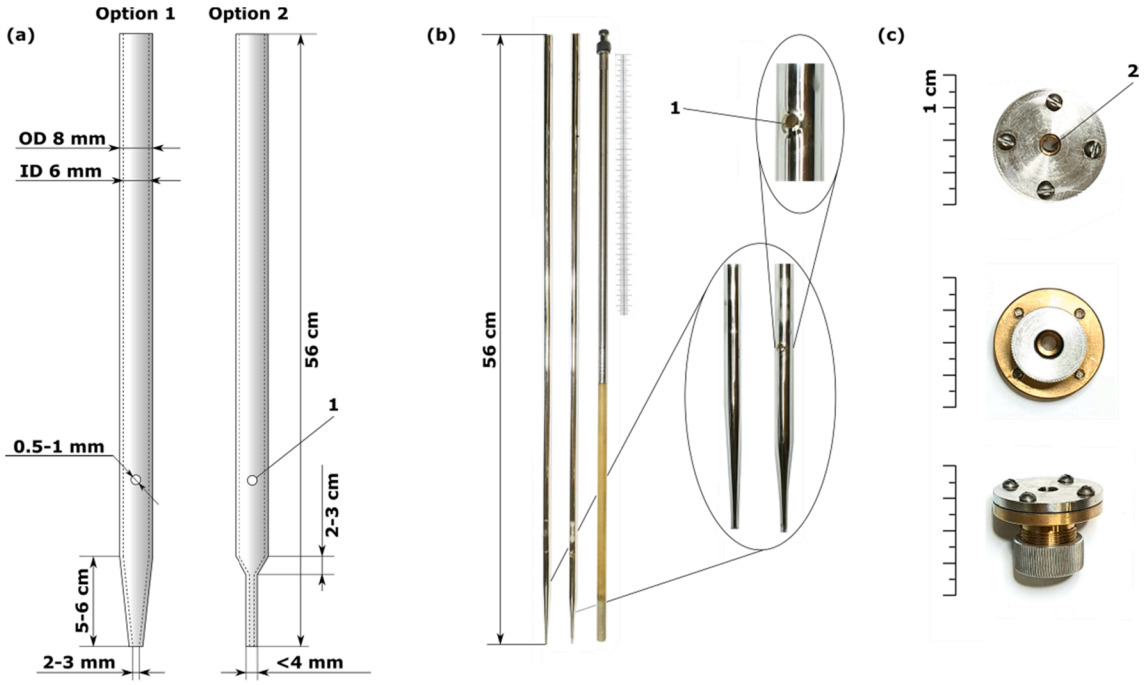

Fig. 2. (a) General scheme of the proposed designs for THz waveguides combined with the EPR sample holder. Proportions are exaggerated. All dimensions except the length of the tapered part (approximately 5–6 cm for option 1 and 2–3 cm for option 2) are the same and shown in the figure for both proposed designs. Number 1 indicates a ventilation hole. (b) Photographs of the waveguides, manufactured according to options 1 and 2, from left to right, respectively, and a standard EPR sample holder for comparison. The insets show the tapered region for both waveguide designs and a more detailed view of the ventilation hole. Number 1 indicates a ventilation hole. (c) Photographs of a cap that is used for cutting off the atmosphere from the inner volume of the cryostat. Number 2 indicates the polypropylene film, which is used for far infrared and terahertz frequency range. A potassium bromide window is used in case of middle infrared range.

3.2. Waveguide material

Optical quartz was used as a material for the developed waveguides. It has low thermal expansion factor, does not affect the properties of the X-band resonator, and can be tapered into a desired shape. The inner surface of the waveguide should be coated by some THz-reflective material, in order to increase the transmission coefficient and protect the internal (lateral) parts of the resonator from high-power THz radiation. The dimensions of the waveguides imply multiple reflections of THz radiation upon propagation and applicability of geometrical (ray) optics for qualitative analysis. Such waveguides are broadband and multimodal; however, multiple reflections significantly affect the polarization properties of radiation (see Results and Discussion). The multimodality allows using the same waveguide in a wide range of frequency that is of great importance for available NovoFEL energy window (1170 cm^{-1} / 8.5 μm – 30 cm^{-1} / 350 μm). Taking into account the need to cover the inner surface of the quartz tube with a conducting material, silver may be a good option. It has low ohmic resistance and can be chemically precipitated on the surface from solution with the possibility to control the quality and thickness of the coating.

3.3. Inner surface silvering

Silvering of the inner surface of the waveguide is usually achieved by the silver mirror reaction. While there is a lot of information concerning the procedure, obtaining a good reflective surface is challenging. There are two main points to consider. First, in order to uniformly cover the surface, the waveguide must be washed very thoroughly. Otherwise, silver falls out in the form of colloidal particles into solution. Second, variability of the layer thickness leads to surface roughness and loss of reflective properties. Having empirically tried about 20 different proportions between silver nitrate and glucose, we established that the silver nitrate should be in a large excess relative to glucose and the reaction time should be about two and a half minutes. The large excess of silver nitrate leads to a fairly rapid reaction, resulting in a uniform coating thickness. In order to achieve a sufficient thickness of the coating, the whole procedure should be repeated 4–5 times. It is also important to note that rinsing the freshly silvered waveguide with diluted ammonia slightly improves the quality of the inner silver surface (visual inspection). The detailed procedures of the reaction as well as preparation are described in the supplementary material.

4. Results and discussion

Using the design and procedure described in the previous section, we manufactured and silvered 15 waveguides. Among them, 7 were selected for further measurements with the best quality of silver coating (checked by visual inspection). The following subsections present a performance study of 10 (including 3 that were used as references) preselected manufactured waveguides, corroborate experimental results by numerical simulations, and discuss future perspectives for the use of the waveguides at the X-band EPR endstation.

4.1. Waveguide performance

The performance of the THz waveguides was characterized by the measurements of the transmission coefficient and the degree of radiation polarization. Four main types of waveguides were used in the measurements: (i) silvered waveguides with gradual tapering (option 1 of Fig. 2a), (ii) silvered waveguides with steep tapering (option 2 of Fig. 2a), (iii) unsilvered (clear quartz) waveguide with steep tapering, (iv) silvered waveguides without tapering (a hollow cylinder of 56 cm length, 8 and 6 mm in outer and inner diameter, respectively) and their unsilvered and brass counterparts. A photograph of the entire set of manufactured waveguides is given in Fig. S6 of the supplementary material.

To measure the transmission coefficient, a waveguide was fixed vertically. THz beam was focused at the entrance of the waveguide by the second off-axis parabolic mirror of the optical system of the EPR endstation [30]. The size of the focused beam at the entrance was less than 2 mm in diameter. The average power of radiation was measured at the entrance (P_{in}) and exit (P_{out}) of the waveguide by Gentec-EO UP19K-15S-VR (Gentec-EO, Canada) power meter. The energies of THz radiation were 45.5 cm^{-1} (220 μm), 77 cm^{-1} (130 μm), 183 cm^{-1} (55 μm), and 1118 cm^{-1} (9 μm) – all of these wavelengths are much smaller than both the focus size and waveguide width. The radiation spectra used are given in the supplementary material. NovoFEL was operated in the power modulation mode [35], in order to decrease the average power at the entrance of the waveguide to approximately 1 W and keep it stable. The transmission coefficient is $T = P_{in}/P_{out}$. Polyethylene far infrared and ZnSe middle infrared polarizers (Bruker Optics, Germany) were used to characterize the remaining polarization of the waveguides. First, the polarization of the FEL radiation was confirmed to be linear. To do thus, we measure the power of THz radiation with the polarizer installed in front of the power meter. The polarizer was placed in two opposite (90°) orientations resulting in maximum and minimum transmission. These measurements confirmed the linear polarization of the NovoFEL radiation. After that, the same procedure was repeated, placing the power meter and polarizer at the exit of the waveguide. The degree of polarization at the exit of the waveguide is $P = (P_{max} - P_{min})/(P_{max} + P_{min})$, where P_{max} and P_{min} are, respectively, correspond to the maximum and minimum average power measured at opposite (90°) orientations of polarizer. In all measurements, a cap (see Fig. 2c) with a polypropylene film (thickness is 30 μm) was fixed at the entrance of the THz waveguide for better similarity with real experimental conditions at X-band EPR endstation. The polypropylene film reduced the overall transmittance by 5–8%, but did not affect polarization degree. The characterization results for all considered waveguides are given in Table 1.

The experimental results presented in Table 1 can be summarized in five main theses: (i) the transmission coefficient decreases with increasing wavenumber (for silvered or brass waveguides), (ii) degree of polarization does not exceed 0.35 for tapered silvered waveguides and further decreases with increasing wavenumber, (iii) tapering has no significant effect on the transmission coefficient of silvered waveguides, (iv) gradual and steep silvered waveguides do not differ in their performance (except for polarization degree at 77 cm^{-1}), (v) silvering increases the transmittance, reaching the transmission efficiency equal to a brass waveguide of the same design.

In more detail, the proposed waveguides 1–6 show high transmission coefficient of up to 0.65 (transmission loss down to 4.4 dB/m) in the THz and far infrared frequency range, achieving the transmittance of untapered waveguides 8 and 10. The transmittance drops significantly in the middle infrared range to the value below 0.10 (loss of 12.5 dB/m). The unsilvered waveguides 7 and 9 have low transmittance, but better conserve the initial radiation polarization. For all silvered waveguides, as well as brass waveguide 10, the radiation at the end of the waveguide is practically unpolarized. The possible reasons of these experimental findings are discussed in the next subsections.

4.2. Qualitative explanation

As mentioned above the waveguides are large compared to the wavelength, thus can be described in the framework of the geometrical optics. The incident Gaussian beam can be considered as a superposition of plane waves with small angles with respect to the waveguide axis, due to relatively large focus size (see the supplementary material for more details). The maximum incidence angle is $\lambda/(\pi w_0)$, where λ is the wavelength and w_0 is the focus radius (< 1 mm). This angle is at most 4° for wavenumber 45.5 cm^{-1} and even smaller for larger wavenumbers. For hollow metallic or metallic-coated waveguides the (intensity) reflection coefficient for any ray is close to 1, but not exactly so due to finite conductivity of metal. More specifically, the absorption during a

Table 1
The performance of manufactured THz waveguides at different wavenumbers.

Waveguide type	Transmission T[a] (transmission loss, dB/m)[b]				Polarization degree P[c]			
	Wavenumber (cm^{-1})				Wavenumber (cm^{-1})			
	45.5	77	183	1118	45.5	77	183	1118
1, gradual[d]	0.64 (4.5)	0.56 (5.0)	0.49 (5.6)	0.10 (12.5)	0.35	0.02	0.03	0.06
2, gradual[d]	0.62 (4.6)	0.53 (5.3)	0.47 (5.8)	0.09 (13.0)	0.31	0.02	0.02	0.10
3, gradual[d]	0.58 (4.9)	0.67 (4.3)	0.49 (5.6)	0.06 (14.7)	0.30	0.03	0.03	0.06
4, steep[e]	0.64 (4.5)	0.58 (4.9)	0.42 (6.3)	0.11 (12.1)	0.35	0.13	0.02	0.06
5, steep[e]	0.62 (4.6)	0.61 (4.7)	0.43 (6.2)	0.12 (11.7)	0.33	0.11	0.02	0.04
6, steep[e]	0.58 (4.9)	0.50 (5.5)	0.43 (6.2)	0.09 (13.0)	0.14	0.17	0.05	0.05
7, steep, unsilvered[f]	0.08 (13.5)	0.14 (11.1)	0.05 (15.5)	0.06 (14.7)	0.57	0.79	0.49[j]	0.19[j]
8, untapered[g]	0.66 (4.3)	0.67 (4.3)	0.63 (4.5)	0.15 (10.8)	0.68	0.03	0.02	0.06
9, untapered, unsilvered[h]	0.16 (10.5)	0.25 (8.6)	0.21 (9.3)	0.17 (10.2)	0.73	0.78	0.72	0.47
10, untapered, brass[i]	0.52 (5.4)	0.61 (4.7)	0.57 (5.0)	0.16 (10.5)	0.10	0.07	0.01	0.27

a, transmission coefficient is given for the entire length of the waveguide (56 cm); **b**, transmission loss in dB/m was calculated from T; **c**, polarization degree at the waveguide exit; **d**, waveguide is manufactured using gradual tapering (option 2 of Fig. 2a) and is silvered according to the described procedure; **e**, waveguide is manufactured using steep tapering (option 1 of Fig. 2a) and is silvered; **f**, unsilvered waveguide with steep tapering; **g**, silvered waveguide without tapering; **h**, unsilvered waveguide without tapering; **i**, brass waveguide without tapering; **j**, the value is unreliable, since the transmission coefficient is low. See the main text for details.

single reflection, and hence the loss coefficient of the whole waveguide, is proportional to the real part of the surface impedance [41], see the supplementary material for details. For non-magnetic materials, it is expressed as:

$$\zeta' = \sqrt{\frac{\mu_0}{\epsilon_0}}\,\frac{n}{n^2+k^2}, \tag{1}$$

where ε_0, μ_0 are vacuum permittivity and permeability, while n and k are real and imaginary parts of the refractive index, respectively. Here we assume that the coating thickness is sufficiently large, which also explains the similar behavior of metal-coated and metal waveguides.

The values of n and k, needed to calculate the surface impedance, are given in ref. [42] for various metals, including silver and copper. Copper was chosen as a metal with comparable conductivity to that of the brass that was used to manufacture waveguide 10. The trend in the behavior of the real part of the surface impedance is expected to be the same for copper and brass. Fig. 3c, 3d show the surface impedance calculated for the same wavelength range using eq. (1). As it can be seen, the surface impedance increases with decreasing the wavelength, resulting in higher losses. The same trend was observed in the experiment, where changing the wavelength from 220 μm to 9 μm causes a decrease in transmittance from about 0.6 to 0.1. It should be noted that qualitative estimate of the absorption loss requires one to estimate the average number of reflections in the waveguide, which depends on the details of the incident beam. However, we expect that the number of reflections actually decreases with the wavelength due to the decreasing average incidence angle with respect to the waveguide axis. Moreover, the surface roughness of the coating may play a role, especially at larger wavenumbers [43,44]. Obviously, the above reasoning applies only to metal or metal-coated waveguides, while for hollow dielectric (unsilvered) waveguides the reflection coefficient is relatively small (even at near-grazing angles) but almost independent of the wavelength, as is the refractive index of the quartz (at least for wavenumbers ≤ 200 cm^{-1} [45]). This is supported by measurements for waveguide 9, and the increase of transmission for wavenumbers 77 and 183 cm^{-1} with respect to 45.5 cm^{-1} can be due to a smaller number of reflections. The largest wavenumber (1118 cm^{-1}) falls into the absorption band for quartz [45], resulting in different performance of the waveguide.

Let us further consider the effect of tapering. All considered tapering angles are small (less than 6°) which, combined with small incidence angles (less than 4°), implies that any incident ray will reach the end of the waveguide (and will not turn back). Note that reflection from the tapering increments the incidence angle (with respect to the waveguide axis) by twice the tapering angle. The number of reflections may increase by one, which does not significantly affect the total transmission coefficient, as long as reflection coefficient weakly depends on the incidence angle (as is the case for metallic surface). This explains why the tapering (of any of the two considered variants) does not significantly affect the transmission coefficient for silver-coated waveguides. The partial exceptions are the results for larger wavenumbers, where the tapering does reduce the transmission, since even a single additional reflection (in addition to relatively small number) is noticeable. Moreover, in this case the intensity reflection coefficient slightly depends on incident angle, as discussed in the supplementary material. But even then there is no significant difference between gradual and steep tapering in full agreement with the qualitative theory. Another obvious

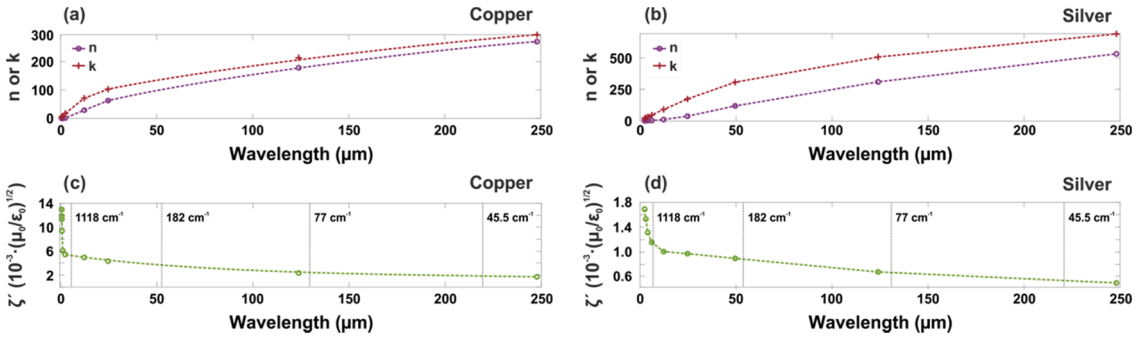

Fig. 3. (a), (b) Dependence of the real (n) and imaginary (k) parts of the refractive index of copper and silver, respectively [42]. (c), (d) Dependence of the real part of the surface impedance of copper and silver, respectively, as the function of the wavelength. The vertical dashed lines show the wavenumbers at which experiments were carried out.

exception is the results for unsilvered waveguides (7 and 9) – here the steep tapering introduces additional reflection with significantly larger angle with respect to the surface, resulting in smaller reflection coefficient (see the supplementary material for details). Moreover, steep tapering leads to a few reflections with angles larger than 12° in the last straight segment of the waveguide (2–3 cm in length).

The discussion of the polarization (even qualitative) is more complicated and is, thus, given in the supplementary material. Here we only summarize the main conclusion. The reflectance from the metal is largely different from that of the dielectric in terms of phase. Most importantly, the two polarizations reflected by an ideal metal differ in sign, which causes depolarization of the wave propagating in the corresponding waveguides. The polarization in a cylindrical metallic waveguide can be conserved when the incident radiation effectively couples to a single or several linearly-polarized modes, but both tapering and, especially, finite conductivity of metal breaks this simple picture. This explains relatively high polarization degree at 45.5 cm^{-1} (especially for untapered waveguide 8) and much smaller values at other wavenumbers. By contrast, unsilvered waveguides do not have this problems – they filter out the near-paraxial components of the incident beam (hence relatively small transmittance), which is propagated with little loss of polarization.

4.3. Simulations

To support the qualitative explanation of the previous subsection, we carried out a numerical simulation of the THz wave propagation in the waveguide. The simulation was done in COMSOL Multiphysics 5.6 using the Radio Frequency, Electromagnetic Waves, Frequency Domain interface. The propagation of a THz wave was calculated through a 20 cm straight section of the waveguide at 45.5 cm^{-1} (220 μm). A silver tube with an inner diameter of 6 mm, the same as in the manufactured waveguides, was used as a model. Only part of the waveguide (20 cm), but not the whole one, was chosen because the calculation of the entire 56 cm waveguide requires too many grid points to be considered, which was not possible for the computer used (two processors with 6 cores and 2.4 GHz each, 256 Gb RAM, for more details see the supplementary material). Since only minor differences were found experimentally between tapered and untapered silvered waveguides, numerical simulations were carried out only for untapered waveguides, which are straight pipes.

4.3.1. Transmittance

To mimic the experimental conditions, the initial distribution of the wave at the entrance to the waveguide was chosen as a focused linearly polarized Gaussian beam 2 mm in diameter. As the boundary conditions on the walls of the waveguide, the impedance boundary condition was used with the refractive index corresponding to the refractive index of silver at wavenumber 45.5 cm^{-1} ($n = 480.9$, $k = 647.7$ [42]). The THz radiation transmission as a function of the distance from the waveguide entrance is shown in Fig. 4.

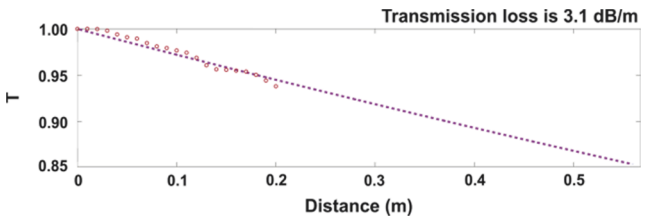

Fig. 4. Calculated dependence of the transmission coefficient (T, red circles) on the distance from the entrance to the waveguide and its exponential fitting (dashed blue line). The propagation of a THz wave was calculated through a straight section of the waveguide with a length of 20 cm at wavenumber 45.5 cm^{-1} (220 μm). The transmittance of the entire waveguide was obtained using an exponential fit extrapolation, and it is equal to 0.85 (3.1 dB/m).

According to Fig. 4, the losses in the waveguide change as a function of distance in a complex way, since the beam propagating in the waveguide consists of many modes with different attenuation constants. Nevertheless, the data were fitted using an exponential curve and the propagation over the entire length of the waveguide was obtained using an extrapolation of the fitting curve. The predicted transmittance of the entire waveguide is about 0.85 (3.1 dB/m). The deviation from the experimental data (see Table 1) can be explained by an additional losses in experiment due to coating roughness [43,44].

4.3.2. Polarization

Numerical simulations of the wave propagation in the straight section of the waveguide unveil the mechanism of almost complete loss of polarization in the proposed THz waveguides. Since the presence of energy losses complicates the qualitative description of polarization losses, the simulation was carried out without them. In this case, the real part of the surface impedance of the waveguide wall was assumed to be zero, as for perfect electric conductor. The incident beam was aligned with the waveguide axis; this allowed us to reduce the problem to an axisymmetric one. After the simulation we reconstructed the field amplitude at each point of the waveguide – the results are shown in Fig. 5a. Fig. 5b, 5c show the direction of the electric field vector in several cross-sections of the waveguide spaced every 40 mm. Two situations are considered, namely when the incident beam has zero phase (Fig. 5b) and when the latter has a phase equal to 90° (Fig. 5c). In the first case an instantaneous value of the electric field of the incident beam is maximum and with a phase shift of 90° this value is zero. Together, these two figures show changes in the polarization of radiation as it passes through the waveguide. For instance, if the phase shift of 90° results only in change of the amplitude of the electric field, the local polarization is linear (although the polarization direction may differ from that of incident beam). If the phase shift of 90° changes the direction of the electric field, the local polarization of the wave is not linear. More specifically, if this change rotates the electric field vector by 90° without changing its amplitude, the local polarization is circular. Otherwise, the local polarization is elliptical.

According to Fig. 5b and 5c, changes in the phase of the incident beam give rise to the rotation of the electric field vector in the cross-sections of the waveguide everywhere except for two coordinate axes. Qualitatively, this can be described as a superposition of at least two modes (with different propagation constants), each having linear polarization along these axes. For instance, this can be modes EH_{11} and EH_{-11} [46], which have maximum amplitudes of the electric field in the center and at 0.59 of radius – similar to the observed distribution of the z–component of the Poynting vector. However, detailed modal analysis is outside of the scope of this paper. Moreover, as discussed in the supplementary material this case is not representative for the polarization properties of tapered waveguides. In these simulations significant fraction of power goes into the EH_{11} mode, which conserves linear polarization. This explains the large polarization degree for waveguide 8 at 45.5 cm^{-1}. By contrast, in the tapering region EH_{11} mode will couple to other modes, leading to additional depolarization. Unfortunately, we are not aware of any simple way to describe this process.

4.4. Mutual orientation of the propagation vector k of the THz wave and magnetic field B_0 of the EPR spectrometer

The experimental and simulation results described in the previous subsections show that the proposed THz waveguides have relatively high radiation transmission coefficients for the NovoFEL frequency range. As an example of their use, we can consider two types of experiments carried out at the EPR endstation in which THz radiation has, respectively, the following characteristics: (i) unpolarized with the radiation propagation vector **k** perpendicular to the B_0 field of the EPR spectrometer, (ii) circularly polarized with the propagation vector **k** parallel to the B_0 field. Geometries when vector **k** is perpendicular or

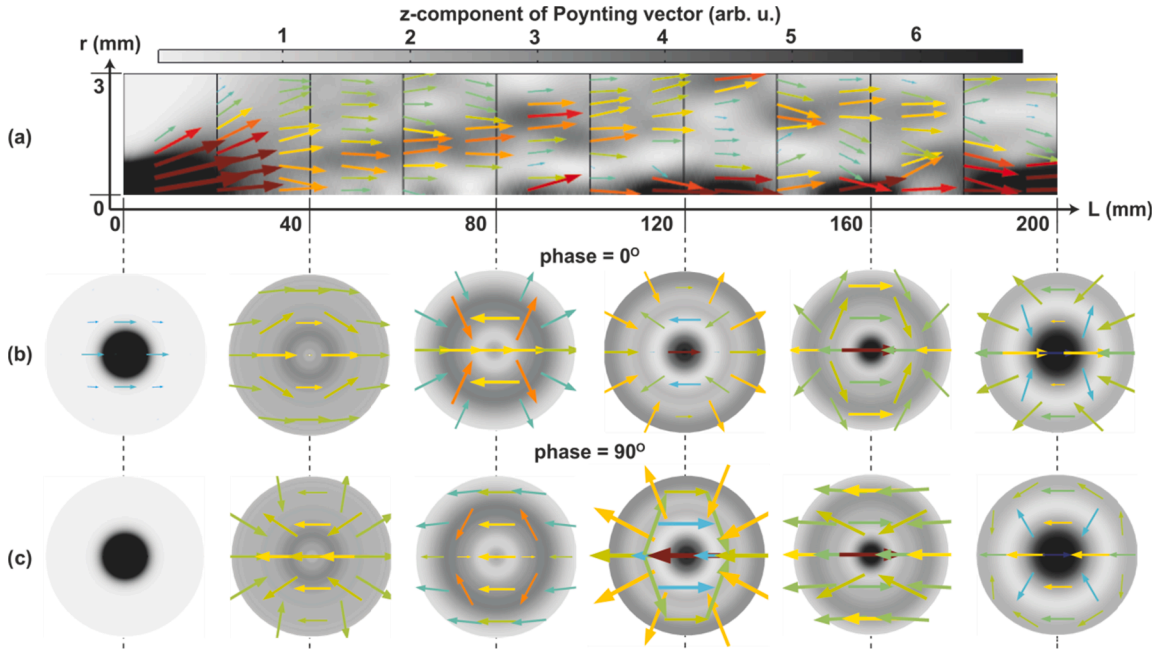

Fig. 5. (a) Poynting vector displayed for 200 mm long straight section of the waveguide. The vertical scale is exaggerated for clarity. The arrows depict both the direction and the amplitude of the Poynting vector and their scale is logarithmic. The colorbar shows the z-component of the Poynting vector (in the linear scale) and is the same for all figures (a)-(c). (b) Electric field vector in several cross-sections of the waveguide spaced every 40 mm in the case when the incident wave has zero phase. The arrows depict both the direction and the amplitude of the electric field vector. The amplitude scale is logarithmic and the same for all parts in (b) and (c). (c) The same as (b) for 90° phase of the incident wave.

parallel to the B_0 field are called Voigt or Faraday geometries, respectively [8]. The configuration (ii) allows selective excitation of spin transitions in high-spin systems [47–49].

EPR measurements with the sample irradiation by unpolarized THz light can be carried out straightforwardly. For this, a sample pellet (4 mm in diameter) or a single crystal should be placed in a thin-walled polyethylene (PE) tube of, e.g., 4 mm in diameter. The PE tube can be fixed at the end of the waveguide using, e.g., parafilm. If necessary, a thin polytetrafluoroethylene film is used as the bottom of the tube. The described method of fixing the sample to the THz waveguide is schematically shown in Fig. 6a. In this case, the radiation propagation vector **k** of THz radiation is perpendicular to the B_0 field of the EPR spectrometer. The distance between the silver-coated end of the waveguide and the sample is about 8–10 mm that is optimal both to avoid the insertion of conducting THz waveguide into the EPR resonator and to uniformly irradiate the sample by THz light.

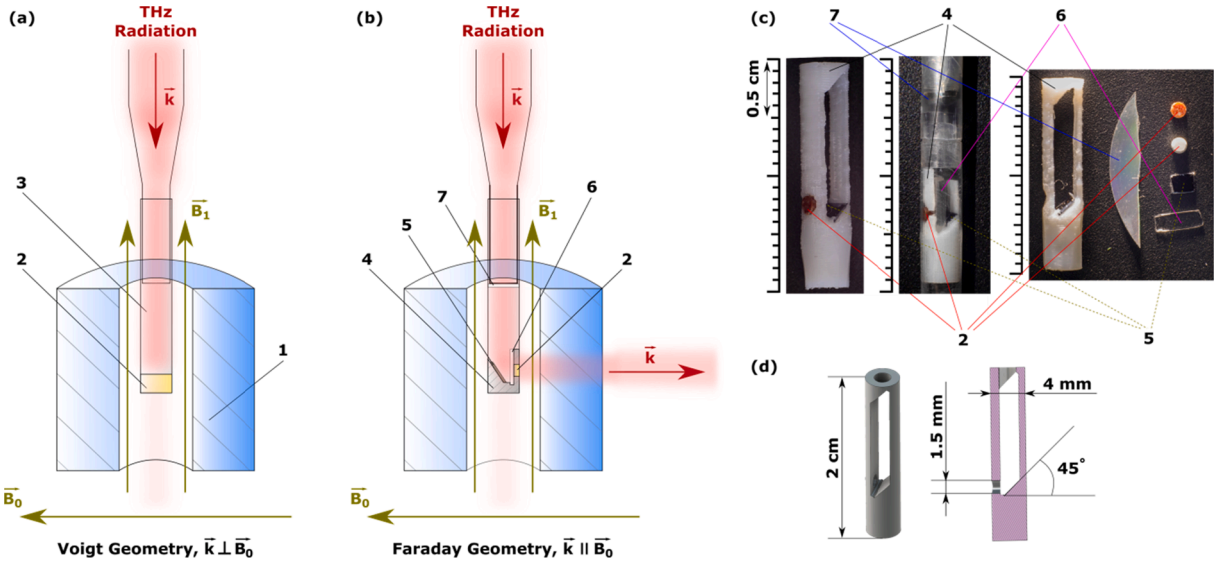

Fig. 6. (a) The method of fixing the sample to the THz waveguide for EPR experiments under unpolarized THz radiation in Voigt geometry, in which the radiation propagation vector perpendicular to the B_0 field of the EPR spectrometer. Proportions are exaggerated. (b) The same as (a) for experiments under polarized radiation in Faraday geometry; the radiation propagation vector is parallel to the B_0 field. (c) From left to right: the photograph of the 3D printed polystyrene insert with a 1.5 mm sample pellet and a silicone plate inside, the photograph of the insert with all assembled components for the experiment in Faraday geometry, and the photograph of the components. (d) Scheme of polystyrene insert with the most critical dimensions. In all figures numbers show: (1) MD-5 sapphire dielectric cylinder, (2) 4 or 1.5 mm ultrahigh-molecular-weight PE pellet of the sample, (3) thin-walled 4 mm PE tube, (4) 3D printed polystyrene insert, (5) rectangular silicon plate of about 2 by 3 mm that is used as a semiconductor mirror, (6) quarter-wave plate, (7) polarizer.

While unpolarized THz radiation can provide insight into the thermal and spin relaxation of various systems using T-jump spectroscopy [30,50–52], resonant circularly polarized THz radiation can in principle be used to manipulate the spin state of single-molecule magnets (SMMs). Ref. [49] proposed an approach, in which circularly polarized alternating magnetic fields in the far infrared or THz range induce selective magnetic dipole transitions between two Kramers doublets of the SMM with the total spin S = 3/2 and subsequent polarized microwave pulses transfer excitation inside the upper Kramers doublet. In order to perform selective excitation of inter-Kramers doublet transitions, i.e. +3/2 ↔ +1/2 or −3/2 ↔ -1/2, one should use Faraday geometry, shown in Fig. 6b, where the radiation propagation vector **k** is parallel to the B_0 magnetic field of the EPR spectrometer [48]. Radiation should be circularly polarized that can be achieved by a polarizer and a quarter-wave plate. Taking into account the proposed waveguide design, THz radiation should be turned through 90° inside the MD-5 sapphire dielectric cylinder. Since the degree of radiation polarization at the waveguide exit is rather low (see Table 1), the polarizer and quarter-wave plate should be placed after the waveguide to restore the linear polarization and further convert it to the circular one, respectively. This implies that these optical elements should be placed in close proximity to the sample.

For this purpose, we printed a polystyrene insert for the EPR resonator, on which a mirror, quarter-wave plate, and the sample can be placed. Polystyrene practically does not affect the properties of the X-band resonator. The polarizer film can be fixed directly at the exit of the waveguide using adhesive tape or parafilm. The schematic representation of the insert is shown in Fig. 6d. The outer diameter of the insert is 4 mm, which allows fixing it in a 4 mm PE tube that is used for experiments in Voigt geometry. There is a 1.5 mm hole on the side wall of the insert for vertical fixing of the sample pellet. The quarter-wave plate is placed into a hollow on the bottom of the insert and glued to the wall by means of polystyrene dissolved in toluene. A mirror can be glued on a 45° bevel located opposite the hole for the sample pellet. The top part of the insert is printed for rigidity and is cut before being fixed in the PE tube for carrying out experiments. The entire assembly, as well as its individual parts, are shown in Fig. 6c.

As a mirror, we use a rectangular silicon plate with dimensions of about 2 by 3 mm, which reflects about 50% of incident radiation in the frequency range of the NovoFEL and does not affect the properties of the X-band resonator. The transmission coefficient of the assembly together with the waveguide is about 0.15 for the far infrared frequency range (30–285 cm^{-1}). Taking into account the high average power of the NovoFEL, achieved transmission coefficient makes it possible to carry out different experiments with circularly polarized pulsed radiation.

5. Conclusions

The obtained results and performed simulations show that the proposed hollow THz waveguides have high transmittance in a wide frequency range, but low efficiency of polarization retention. The design of the waveguides is tailored for their use in conditions of a highly limited aperture of the EPR probehead and allows radiation to be transferred over the distances of about 60 cm with moderate losses. The waveguide has a form of long hollow cylinder tapering towards the end. The 6 mm inner diameter implies multiple reflection of the THz radiation from the waveguide surfaces, demanding the latter be chemically coated by silver. The two possible design options, namely with a steeper (approximately 2–3 cm) or more gradual (approximately 5–6 cm) tapering region show practically identical performance. In both cases the transmission coefficient decreases with increasing wavenumber from about 0.65 (4.4 dB/m) at 45.5 cm^{-1} (220 μm) to about 0.10 (12.5 dB/m) at 1118 cm^{-1} (9 μm), which can be rationalized by an increase of the surface impedance of the silvered waveguide with decreasing wavelength. The measured transmittance of the waveguides is comparable with the transmittance of a brass waveguide of the same design at all energies used. The polarization degree of transmitted radiation decreases substantially after passing through the waveguides. The highest output polarization degree for tapered waveguides was at the level of 0.35 for the wavenumber 45.5 cm^{-1}. The loss of the initial linear polarization of the beam during its propagation along the waveguide was confirmed both by qualitative geometrical-optics discussion and by the numerical simulations.

The proposed waveguide design is flexible enough for further modifications and can be used for other setups with different spatial constraints and waveguide-shape requirements. In case of the EPR spectroscopy, the relative orientation of the radiation propagation vector **k** and the static magnetic field B_0 is of particular importance. Miniature insert consisting of THz polarizer, mirror and quarter-wave plate was developed in order to achieve the alignment of **k** with B_0 and transform the linear polarization to the circular one inside the EPR probehead. The overall transmission coefficient of the miniature insert together with the waveguide is about 0.15 making it possible to carry out EPR experiments using circularly polarized high-power pulsed radiation.

CRediT authorship contribution statement

Anatoly R. Melnikov: Investigation, Data curation, Writing - original draft. **Arkady A. Samsonenko:** Investigation, Formal analysis, Writing - review & editing. **Yaroslav V. Getmanov:** Resources. **Oleg A. Shevchenko:** Resources. **Darya A. Shevchenko:** Resources. **Alexander A. Stepanov:** Resources. **Matvey V. Fedin:** Writing - review & editing, Project administration. **Maxim A. Yurkin:** Formal analysis, Validation, Writing - review & editing. **Sergey L. Veber:** Writing - original draft, Conceptualization, Supervision, Funding acquisition.

Declaration of competing interest

The authors declare that they have no known competing financial interests or personal relationships that could have appeared to influence the work reported in this paper.

Acknowledgments

The development of broadband multimodal THz waveguides and their characterization at the NovoFEL facility were funded by the Russian Science Foundation, grant number 17-13-01412. A.R.M. is grateful to the Council for Grants of the President of the Russian Federation for awarding a personal scholarship for Support of Young Researchers (Project No. SP-272.2021.5). We also thank Iryna Synelnyk for insightful discussion of waveguide theory.

Appendix A. Supplementary material

Supplementary data to this article can be found online at https://doi.org/10.1016/j.optlastec.2021.107375.

References

[1] A. Redo-Sanchez, X. Zhang, Terahertz science and technology trends, IEEE J. Sel. Top. Quantum Electron 14(2) (2008) 260-269. doi. 10.1109/JSTQE.2007.913959.
[2] S.S. Dhillon, M.S. Vitiello, E.H. Linfield, A.G. Davies, M.C. Hoffmann, J. Booske, C. Paoloni, M. Gensch, P. Weightman, G.P. Williams, E. Castro-Camus, D.R.S. Cumming, F. Simoens, I. Escorcia-Carranza, J. Grant, S. Lucyszyn, M. Kuwata-Gonokami, K. Konishi, M. Koch, C.A. Schmuttenmaer, T.L. Cocker, R. Huber, A.G. Markelz, Z.D. Taylor, V.P. Wallace, J. Axel Zeitler, J. Sibik, T.M. Korter, B. Ellison, S. Rea, P. Goldsmith, K.B. Cooper, R. Appleby, D. Pardo, P.G. Huggard, V. Krozer, H. Shams, M. Fice, C. Renaud, A. Seeds, A. Stöhr, M. Naftaly, N. Ridler, R. Clarke, J. E. Cunningham, M.B. Johnston, The 2017 terahertz science and technology roadmap, J. Phys. D: Appl. Phys. 50(4) (2017) 043001. Doi. 10.1088/1361-6463/50/4/043001.
[3] X.C. Zhang, A. Shkurinov, Y. Zhang, Extreme terahertz science, Nature Photon 11 (1) (2017) 16-18. Doi: 10.1038/nphoton.2016.249.

[4] D.M. Mittleman, Perspective: Terahertz science and technology, J. Appl. Phys. – 2017. – Vol. 122. – №. 23. – P. 230901. – 10.1063/1.5007683.

[5] V.V. Kubarev, G.I. Sozinov, M.A. Scheglov, A.V. Vodopyanov, A.V. Sidorov, A.R. Melnikov, S.L. Veber, The Radiation Beamline of Novosibirsk Free-Electron Laser Facility Operating in Terahertz, Far-Infrared, and Mid-Infrared Ranges, IEEE T. THz Sci. Techn. 10(6) (2020) 634-646. doi: 10.1109/TTHZ.2020.3010046.

[6] A. Schnegg, J. Behrends, K. Lips, R. Bittl, K. Holldack, Frequency domain Fourier transform THz-EPR on single molecule magnets using coherent synchrotron radiation, Phys. Chem. Chem. Phys.11(31) (2009) 6820-6825. doi 10.1039/B905745E.

[7] J. Telser, J. Krzystek, A. Ozarowski, High-frequency and high-field electron paramagnetic resonance (HFEPR): a new spectroscopic tool for bioinorganic chemistry, J. Biol. Inorg. Chem. 19(3) (2014) 297-318. doi: 10.1007/s00775-013-1084-3.

[8] J. Nehrkorn, K. Holldack, R. Bittl, A. Schnegg, Recent progress in synchrotron-based frequency-domain Fourier-transform THz-EPR, J. Magn. Reson.280 (2017) 10-19. doi: https://doi.org/10.1016/j.jmr.2017.04.001.

[9] G. Gallot, S.P. Jamison, R.W. McGowan, D. Grischkowsky, Terahertz waveguides, J. Opt. Soc. Am. B. 17(5) (2000) 851-863. doi: 10.1364/JOSAB.17.000851.

[10] S.P. Jamison, McGowan R.W., Grischkowsky D. Single-mode waveguide propagation and reshaping of sub-ps terahertz pulses in sapphire fibers, Appl. Phys. Lett. 76(15) 2000 1987-1989. doi: 10.1063/1.126231.

[11] R. Mendis, D. Grischkowsky, Undistorted guided-wave propagation of subpicosecond terahertz pulses, Opt. Lett. – 26(11) (2001) 846-848. doi: 10.1364/OL.26.000846.

[12] K. Wang, D.M. Mittleman, Metal wires for terahertz wave guiding, Nature. 432 (7015) (2004) 376-379. doi: 10.1038/nature03040.

[13] L.-J. Chen, H.-W. Chen, T.-F. Kao, J.-Y. Lu, C.-K. Sun, Low-loss subwavelength plastic fiber for terahertz waveguiding, Opt. Lett. 31(3) (2006) 308-310. doi: 10.1364/OL.31.000308.

[14] R. Wallis, R.D. Innocenti, D.S. Jessop, O. Mitrofanov, C.M. Bledt, J.E. Melzer, J.A. Harrington, H.E. Beere, D.A. Ritchie, Investigation of hollow cylindrical metal terahertz waveguides suitable for cryogenic environments, Opt. Express. 46(26) (2016) 30002-30014. doi: 10.1364/OE.24.030002.

[15] P. Padhy, P.K. Sahu, R. Jha, Metal wire waveguide based all plasmonic refractive index sensor for terahertz frequencies, Sens. Actuat. B Chem. 225 (2016) 115-120. doi: 10.1016/j.snb.2015.09.005.

[16] S. Atakaramians, V.S. Afshar, T.M. Monro, D. Abbott, Terahertz dielectric waveguides, Adv. Opt. Photonics. 5(2) (2013) 169-215. doi: 10.1364/AOP.5.000169.

[17] H. Bao, K. Nielsen, O. Bang, P.U. Jepsen, Dielectric tube waveguides with absorptive cladding for broadband, low-dispersion and low loss THz guiding, Sci. Rep. 5(1) (2015) 7620. doi: 10.1038/srep07620.

[18] A. Meyer, K. Krüger, M. Schneider, Dispersion-minimized rod and tube dielectric waveguides at W-band and D-band frequencies, IEEE Microw. Wirel. Compon. Lett. 28(7) (2018) 555-557. doi: 10.1109/LMWC.2018.2839649.

[19] Y. Zhong, G. Xie, F. Mao, J. Ding, F. Yue, S. Chen, X. Lu, C. Jing, J. Chu, Thin-wall cyclic olefin copolymer tube waveguide for broadband terahertz transmission, Opt. Mater. 98 (2019) 109490. doi: 10.1016/j.optmat.2019.109490.

[20] C.M. Bledt, J.E. Melzer, J.A. Harrington, Fabrication and characterization of improved Ag/PS hollow-glass waveguides for THz transmission, Appl. Opt. 52(27) 2013 6703-6709. doi: 10.1364/AO.52.006703.

[21] M. Navarro-Cía, J.E. Melzer, J.A. Harrington, O. Mitrofanov, Silver-coated teflon tubes for waveguiding at 1–2 THz, J. Infrared Millim. Terahertz Waves. 36 (6) (2015) 542-555. doi: 10.1007/s10762-015-0157-5.

[22] K. Wang, Q. Cao, H. Zhang, P. Shen, L. Xing, Evanescent resonant mode for a T-shaped cavity in a terahertz parallel-plate waveguide, Appl. Opt. 57(27) (2018). doi: 10.1364/AO.57.007967.

[23] K. Jia, L. Fan, Z. Cao, THz narrow band-pass filter based on stopband modulation in corrugated parallel plate waveguides, Opt. Commun. 465 (2020) 125604. doi: 10.1016/j.optcom.2020.125604.

[24] H. Li, S.-g. Li, J.-S. Li, W. Zhang, G.-W. An, Broadband single-polarization single-mode photonic crystal fibers with three different background materials, Appl. Opt. 54(10) (2015) 2851-2856. doi: 10.1364/AO.54.002851.

[25] C. Liu, W. Su, Q. Liu, X. Lu, F. Wang, T. Sun, P.K. Chu, Symmetrical dual D-shape photonic crystal fibers for surface plasmon resonance sensing, Opt. Express. 26(7) 2018 9039-9049. doi: 10.1364/OE.26.009039.

[26] M. Alexander Schmidt, A. Argyros, F. Sorin, Hybrid optical fibers – an innovative platform for in-fiber photonic devices, Adv. Opt. Mater. 4(1) 2016 13-36. doi: 10.1002/adom.201500319.

[27] H. Li, S. Atakaramians, R. Lwin, X. Tang, Z. Yu, A. Argyros, B.T. Kuhlmey, Flexible single-mode hollow-core terahertz fiber with metamaterial cladding, Optica. 3(9) 2016 941–947. doi: 10.1364/OPTICA.3.000941.

[28] J. Melzer, M. Navarro-Cía, O. Mitrofanov, J. Harrington, Silver-coated Teflon hollow waveguides for the delivery of terahertz radiation, SPIE – 2014. – 89380I P.

[29] G. Xie, Y. Zhong, G. Li, C. She, X. Lu, F. Yue, S. Liu, C. Jing, Y. Cheng, J. Chu, 300 GHz bending transmission of silver/polypropylene hollow terahertz waveguide, Results Phys. – 19 (2020) 103534. doi: 10.1016/j.rinp.2020.103534.

[30] S.L. Veber, S.V. Tumanov, E.Y. Fursova, O.A. Shevchenko, Y.V. Getmanov, M.A. Scheglov, V.V. Kubarev, D.A. Shevchenko, I.I. Gorbachev, T.V. Salikova, G.N. Kulipanov, V.I. Ovcharenko, M.V. Fedin, X-band EPR setup with THz light excitation of Novosibirsk Free Electron Laser: Goals, means, useful extras, J. Magn. Reson. 288 (2018) 11-22. Doi:10.1016/j.jmr.2018.01.009.

[31] A.R. Melnikov, M.A. Kiskin, Y.V. Getmanov, O.A. Shevchenko, M.V. Fedin, S.L. Veber, Technical and software improvements of the EPR spectroscopy endstation at the NovoFEL facility: Status 2020, AIP Conf. Proc. 2299(1) (2020) 030010. doi: 10.1063/5.0030338.

[32] G.N. Kulipanov, E.G. Bagryanskaya, E.N. Chesnokov, Y.Y. Choporova, V.V. Gerasimov, Y.V. Getmanov, S.L. Kiselev, B.A. Knyazev, V.V. Kubarev, S.E. Peltek, V.M. Popik, T.V. Salikova, M.A. Scheglov, S.S. Seredniakov, O.A. Shevchenko, A.N. Skrinsky, S.L. Veber, N.A. Vinokurov, Novosibirsk Free Electron Laser - Facility Description and Recent Experiments, IEEE T. THz Sci. Techn. 5(5) (2015) 798-809. doi: 10.1109/TTHZ.2015.2453121.

[33] O.A. Shevchenko, V.S. Arbuzov, N.A. Vinokurov, P.D. Vobly, V.N. Volkov, Y.V. Getmanov, Y.I. Gorbachev, I.V. Davidyuk, O.I. Deychuly, E.N. Dementyev, B.A. Dovzhenko, B.A. Knyazev, E.I. Kolobanov, A.A. Kondakov, V.R. Kozak, E.V. Kozyrev, V.V. Kubarev, G.N. Kulipanov, E.A. Kuper, I.V. Kuptsov, G.Y. Kurkin, S.A. Krutikhin, L.E. Medvedev, S.V. Motygin, V.K. Ovchar, V.N. Osipov, V.M. Petrov, A. M. Pilan, V.M. Popik, V.V. Repkov, T.V.Salikova, I.K. Sedlyarov, S.S. Serednyakov, A.N. Skrinsky, S.V. Tararyshkin, A.G. Tribendis, V.G. Tcheskidov, K.N. Chernov, M. A. Scheglov, The Novosibirsk Free Electron Laser – Unique Source of Terahertz and Infrared Coherent Radiation, Phys. Procedia. 84 (2016) 13-18. doi: 10.1016/j.phpro.2016.11.004.

[34] O.A. Shevchenko, N.A. Vinokurov, V.S. Arbuzov, K.N. Chernov, O.I. Deichuly, E.N. Dementyev, B.A. Dovzhenko, Y.V. Getmanov, Y.I. Gorbachev, B.A. Knyazev, A.A. Kondakov, V.R. Kozak, E.V. Kozyrev, S.A. Krutikhin, V.V. Kubarev, G.N. Kulipanov, E.A. Kuper, I.V. Kuptsov, G.Y. Kurkin, L.E. Medvedev, S.V. Motygin, V.K. Ovchar, V.N. Osipov, V.M. Petrov, A.M. Pilan, V.M. Popik, V.V. Repkov, T.V. Salikova, M.A. Scheglov, I.K. Sedlyarov, S.S. Serednyakov, A.N. Skrinsky, S.V. Tararyshkin, A.G. Tribendis, V.G. Tcheskidov, V.N. Volkov, The Novosibirsk free electron laser facility, AIP Conf. Proc. 2299(1) (2020) 020001. Doi:10.1063/5.0031513.

[35] O.A. Shevchenko, A.R. Melnikov, S.V. Tararyshkin, Y.V. Getmanov, S.S. Serednyakov, E.V. Bykov, V.V. Kubarev, M.V. Fedin, S.L. Veber, Electronic modulation of THz radiation at NovoFEL: Technical aspects and possible applications, Materials. 12(19) 2019 3063. doi: 10.3390/ma12193063.

[36] Y. Twig, E. Suhovoy, A. Blank, Sensitive surface loop-gap microresonators for electron spin resonance, Rev. Sci. Instrum. 81(10) (2010) 104703. doi 10.1063/1.3488365.

[37] M. Dutka, T. Oleś, M. Mossakowski, W. Froncisz, Rectangular loop-gap resonator with the light access to the sample, J. Magn. Reson. 210(1) (2011) 44–50. doi: 10.1016/j.jmr.2011.02.009.

[38] M.Y. Ivanov, V.A. Nadolinny, E.G. Bagryanskaya, Y.A. Grishin, M.V. Fedin, S.L. Veber, Bismuth germanate as a perspective material for dielectric resonators in EPR spectroscopy, J. Magn. Reson. 271 (2016) 83-89. doi: 10.1016/j.jmr.2016.08.009.

[39] V.N. Syryamina, A.G. Matveeva, Y.V. Vasiliev, A. Savitsky, Y.A. Grishin, Improving B1 field homogeneity in dielectric tube resonators for EPR spectroscopy via controlled shaping of the dielectric insert, J. Magn. Res. 311 (2020) 106685. doi: 10.1016/j.jmr.2020.106685.

[40] D. Grischkowsky, S. Keiding, M. van Exter, C. Fattinger, Far-infrared time-domain spectroscopy with terahertz beams of dielectrics and semiconductors, J. Opt. Soc. Am. B. 7(10) (1990) 2006-2015. doi 10.1364/JOSAB.7.002006.

[41] L.D. Landau, E.M. Lifshifs, Electrodynamics of continuous media, by L. D. Landau and E. M. Lifshitz. Translated from the Russian by J. B. Sykes and J. S. Bell, Pergamon Press, Oxford, 1960, p. 417.

[42] H.J. Hagemann, W. Gudat, C. Kunz, Optical constants from the far infrared to the x-ray region: Mg, Al, Cu, Ag, Au, Bi, C, and Al2O3, J. Opt. Soc. Am. 65(6) (1975) 742-744. doi: 10.1364/JOSA.65.000742.

[43] X. Ma, J.S. Ochoa, A.C. Cangellaris, A method for modeling the impact of conductor surface roughness on waveguiding properties of interconnects, in: 2013 IEEE 22nd Conference on Electrical Performance of Electronic Packaging and Systems, 2013, pp. 11–14.

[44] X. Ma, Modeling of conductor surface roughness effect, Master Thesis, Urbana, Illinois, 2014. P. 38.

[45] R. Kitamura, L. Pilon, M. Jonasz, Optical constants of silica glass from extreme ultraviolet to far infrared at near room temperature, Appl. Opt. 2007. 33(46) 8118-8133. 10.1364/AO.46.008118.

[46] E.A.J. Marcatili, R.A. Schmeltzer, Hollow metallic and dielectric waveguides for long distance optical transmission and lasers, Bell Syst. Tech. J. 43(4) (1964) 1783-1809. doi: 10.1002/j.1538-7305.1964.tb04108.x.

[47] L. Sorace, W. Wernsdorfer, C. Thirion, A.L. Barra, M. Pacchioni, D. Mailly, B. Barbara, Photon-assisted tunneling in a Fe8 single-molecule magnet, Phys. Rev. B. 68(22) 2003 220407. doi: 10.1103/PhysRevB.68.220407.

[48] J. van Slageren, S. Vongtragool, A. Mukhin, B. Gorshunov, M. Dressel, Terahertz Faraday effect in single molecule magnets, Phys. Rev. B. 72(2) (2005) 020401. doi: 10.1103/PhysRevB.72.020401.

[49] A.G. Maryasov, M.K. Bowman, M.V. Fedin, S.L. Veber, Theoretical basis for switching a kramers single molecular magnet by circularly-polarized radiation, Materials. 12(23) 2019 3865. doi: 10.3390/ma12233865.

[50] H. Staerk, G. Czerlinski, Nanosecond Heating of Aqueous Systems by Giant Laser Pulses, Nature. 205(4966) (1965) 63-64. doi: 10.1038/205063a0.

[51] J. Kubelka, Time-resolved methods in biophysics. 9. Laser temperature-jump methods for investigating biomolecular dynamics, Photochem. Photobiol. Sci. 8(4) 2009:499-512. doi: 10.1039/B819929A.

[52] E.G. Panarelli, P. Gast, E.J.J. Groenen, Temperature-cycle electron paramagnetic resonance, Phys. Chem. Chem. Phys. 22(17) (2020) 9487-9493. doi: 10.1039/D0CP00664E.